Preprint typeset using LaTeX style emulateapj v. 10/09/06

arXiv:1302.5172v1 [astro-ph.CO] 21 Feb 2013

# VALIDITY OF HYDROSTATIC EQUILIBRIUM IN GALAXY CLUSTERS FROM COSMOLOGICAL HYDRODYNAMICAL SIMULATIONS

Daichi Suto[1], Hajime Kawahara[2], Tetsu Kitayama[3], Shin Sasaki[2],
Yasushi Suto[1,4,5] and Renyue Cen[5]

## ABSTRACT

We examine the validity of the hydrostatic equilibrium (HSE) assumption for galaxy clusters using one of the highest-resolution cosmological hydrodynamical simulations. We define and evaluate several *effective* mass terms corresponding to the Euler equations of the gas dynamics, and quantify the degree of the validity of HSE in terms of the mass estimate. We find that the mass estimated under the HSE assumption (the HSE mass) deviates from the true mass by up to $\sim 30$ %. This level of departure from HSE is consistent with the previous claims, but our physical interpretation is rather different. We demonstrate that the inertial term in the Euler equations makes a negligible contribution to the total mass, and the overall gravity of the cluster is balanced by the thermal gas pressure gradient and the gas acceleration term. Indeed the deviation from the HSE mass is well explained by the acceleration term at almost all radii. We also clarify the confusion of previous work due to the inappropriate application of the Jeans equations in considering the validity of HSE from the gas dynamics extracted from cosmological hydrodynamical simulations.

*Subject headings:* cosmology: theory – galaxies: clusters: general – methods: numerical – X-rays: galaxies: clusters

## 1. INTRODUCTION

Clusters of galaxies are important sources of various cosmological and astrophysical information especially on the formation history of the large scale structure and the estimates of cosmological parameters (Allen et al. 2011, for a recent review). Among others, mass of clusters is one of the most fundamental quantities in virtually all studies. The most conventional method is based on X-ray observations of the intracluster medium (ICM) combined with the assumption that the ICM is in hydrostatic equilibrium (HSE) with the total gravity of the cluster (We call the mass estimated by this method “the HSE mass”). It is unlikely, however, that the HSE assumption strictly holds, especially for unrelaxed clusters given their on-going dynamical evolution. Therefore it is important to examine the validity of the HSE assumption, which has been mostly assumed just for simplicity. The quantitative analysis of its validity and limitation is directly related to the applicability to the future scientific opportunities, including upcoming X-ray missions such as extended Röntgen Survey with Imaging Telescope Array[6] (eROSITA) and ASTRO-H[7], and observations of the Sunyaev-Zel’dovich effect performed by Atacama Cosmology Telescope[8] (ACT) and South Pole Telescope[9] (SPT).

The validity of the HSE assumption for observed clusters may be examined in a straightforward fashion by comparison of the HSE mass with the cluster mass estimated by other methods. In this respect, gravitational lensing is particularly suited because it directly probes the total gravitational mass without any assumption on the dynamical state of dark matter. On the other hand, the lensing observations require a high angular resolution of the background galaxy images and are feasible only for a limited number of clusters located at $z \lesssim 0.5$. In addition, the estimated lensing mass correspond to the cylindrical mass along the line of sight, and may include an extra contribution not associated with the cluster itself. Previous studies (e.g., Mahdavi et al. 2008; Zhang et al. 2008, for recent ones) show that the HSE mass is smaller by approximately 20 percent on average than the lensing mass, suggesting either HSE or lensing, or even both, should be systematically biased.

Another method to examine the validity of the HSE assumption that we pursue in this paper is to use numerical simulations, which enable us to make a detailed and critical comparison of the simulated data against the model prediction. Therefore we can locate the origin of systematic bias, if any, of the HSE assumption. This is useful because we may be able to apply the correction to the observational data eventually.

Of course there are a number of previous studies of HSE using simulated clusters, but their results do not seem to be converged. For instance, let us focus on a couple of recent papers (Fang et al. 2009; Lau et al. 2009) that studied

---

Electronic address: daichi@utap.phys.s.u-tokyo.ac.jp
[1] Department of Physics, The University of Tokyo, Tokyo 113-0033, Japan
[2] Department of Physics, Tokyo Metropolitan University, Hachioji, Tokyo 192-0397, Japan
[3] Department of Physics, Toho University, Funabashi, Chiba 274-8510, Japan
[4] Research Center for the Early Universe, School of Science, The University of Tokyo, Tokyo 113-0033, Japan
[5] Princeton University Observatory, Princeton, NJ 08544

[6] http://www.mpe.mpg.de/eROSITA

[7] http://astro-h.isas.jaxa.jp

[8] http://www.princeton.edu/act

[9] http://pole.uchicago.edu

systematic errors in the HSE mass using the *same* set of 16 clusters simulated by Nagai et al. (2007). Fang et al. (2009) analyzed the gas particle data on the basis of the Euler equations, and evaluated the *effective* mass terms corresponding to several different terms in the equations. Lau et al. (2009) performed basically the same analysis, but used the Jeans equations instead of the Euler equations despite the fact that they considered the gas particles in the simulated clusters. Both reached the similar conclusion that the HSE mass underestimates the true mass of clusters systematically by $\sim$ 10–20 %. Nevertheless their physical interpretations of the origin of the bias are very different; Fang et al. (2009) claimed that the coherent rotation of gas plays a significant role as an additional support against the gravity, while Lau et al. (2009) concluded that the random gas motion is responsible for the departure from HSE, and the gas rotation makes a relatively negligible contribution.

The purpose of the present paper is to clarify the theoretical method to examine HSE of the simulated clusters, and then to revisit its validity using a high-resolution hydrodynamical simulation by Cen (2012). In particular, we compare the two different analysis formulations adopted by Fang et al. (2009) and Lau et al. (2009), and argue that the Euler equations, rather than the Jeans equations modified by a gas pressure gradient term (Rasia et al. 2004; Lau et al. 2009), should be used in analyzing the gas dynamics.

The rest of the paper is organized as follows. Section 2 formulates our method to evaluate the validity of the HSE assumption. We pay a particular emphasis on the comparison between the Euler and Jeans equations in analyzing the gas dynamics. The derivation of those sets of equations starting from the Boltzmann equations is summarized in Appendix A. Section 3 briefly describes the simulated cluster, and then presents our analysis results of the validity of HSE. Finally our conclusion is summarized in Section 4. The analysis based on the Jeans equations using dark matter particles is shown in Appendix B.

## 2. THEORETICAL FORMULATION

### 2.1. *Method to Examine the Validity of HSE based on the Euler Equations*

Our analysis method to discuss the validity of HSE using gas in a simulated cluster is based on the Euler equations:

$$\frac{\partial \boldsymbol{v}}{\partial t} + (\boldsymbol{v}\cdot\nabla)\boldsymbol{v} = -\frac{1}{\rho_{\rm gas}}\nabla p - \nabla\phi, \tag{1}$$

where $\phi$ is the gravitational potential, and $\rho_{\rm gas}$, $\boldsymbol{v}$ and $p$ are the density, velocity and pressure of gas. While the Jeans equations do not describe the gas dynamics in their original form, Rasia et al. (2004) and Lau et al. (2009) added the gas pressure gradient term to the Jeans equations, and adopted the resulting equations in analyzing simulated clusters. We argue in the next subsection that this is not justified, and present the result based on the Jeans equations but using collisionless dark matter particles in Appendix B, for reference.

We define the total mass $M_{\rm tot}$ of a cluster inside a volume $V$ as

$$M_{\rm tot} = \int_V d^3x\ \rho_{\rm tot}, \tag{2}$$

where $\rho_{\rm tot}$ is the total density of the cluster. For the simulated cluster considered throughout this paper, $\rho_{\rm tot}$ consists of densities of gas, dark matter and stars, i.e., $\rho_{\rm tot} = \rho_{\rm gas} + \rho_{\rm dm} + \rho_{\rm star}$. The total mass can be rewritten in terms of $p$ and $\boldsymbol{v}$ using Poisson's equation and Gauss's theorem:

$$M_{\rm tot} = \frac{1}{4\pi G}\int_{\partial V} d\boldsymbol{S}\cdot\nabla\phi = \frac{1}{4\pi G}\int_{\partial V} d\boldsymbol{S}\cdot\left[-\frac{1}{\rho_{\rm gas}}\nabla p - (\boldsymbol{v}\cdot\nabla)\boldsymbol{v} - \frac{\partial \boldsymbol{v}}{\partial t}\right], \tag{3}$$

where $\partial V$ is the surface surrounding the volume $V$ and we have used equation (1) in the second equality. Now the total mass is evaluated by the gas quantities alone, without any knowledge on dark matter and stars. This is why the present method is applicable, in principle, to the X-ray data of galaxy clusters.

If we adopt a spherical surface as $\partial V$, the total mass can be decomposed into the following four *effective* mass terms:

$$M_{\rm tot} = M_{\rm therm} + M_{\rm rot} + M_{\rm stream} + M_{\rm accel}, \tag{4}$$

where

$$M_{\rm therm} = -\frac{1}{4\pi G}\int_{\partial V} dS\ \frac{1}{\rho_{\rm gas}}\frac{\partial p}{\partial r}, \tag{5}$$

$$M_{\rm rot} = \frac{1}{4\pi G}\int_{\partial V} dS\ \frac{v_\theta^2 + v_\varphi^2}{r}, \tag{6}$$

$$M_{\rm stream} = -\frac{1}{4\pi G}\int_{\partial V} dS\ \left[v_r\frac{\partial v_r}{\partial r} + \frac{v_\theta}{r}\frac{\partial v_r}{\partial \theta} + \frac{v_\varphi}{r\sin\theta}\frac{\partial v_r}{\partial \varphi}\right], \tag{7}$$

and

$$M_{\rm accel} = -\frac{1}{4\pi G}\int_{\partial V} dS\ \frac{\partial v_r}{\partial t}. \tag{8}$$

We emphasize here that the above set of equations does not assume spherical symmetry of the system; we just take a spherical surface as the integral surface and write down equation (3) in spherical coordinates.

The first term, $M_{\rm therm}$, originates from the thermal pressure gradient of gas. If the gas motion is negligible, $M_{\rm therm}$ should be equal to the total mass $M_{\rm tot}$, and thus regarded as a cluster mass estimated under the HSE assumption. In other words, the difference between $M_{\rm tot}$ and $M_{\rm therm}$ is a quantitative measure of the departure from the HSE assumption.

The inertial term $(\boldsymbol{v} \cdot \nabla)\boldsymbol{v}$ in the Euler equations reduces to $M_{\rm rot}$ and $M_{\rm stream}$. If there exists a coherent rotational motion around the center of the cluster, $M_{\rm rot}$ can be interpreted as the centrifugal force term. Without such a motion, however, the local tangential velocity of different directions at different locations on the sphere could make $M_{\rm rot}$ significantly large. During the course of the cluster evolution, gas generally falls toward the center of the cluster with larger streaming speed with increasing radius from the center. In this case, $M_{\rm stream}$ becomes *negative* and cannot be neglected. On the other hand, it becomes positive and/or negligible, especially in the innermost region where the gas velocity is more randomized than that in the outer regions.

Finally the acceleration term, $M_{\rm accel}$, corresponds to the $-\partial v_r/\partial t$ term in the Euler equations, and becomes positive/negative when gas is decelerating/accelerating.

All the mass terms are invariant with respect to the choice of the axis of the spherical coordinates, but are not necessarily positive. Note also that $M_{\rm rot}$ and $M_{\rm stream}$, corresponding to the inertial term, are not invariant with respect to the Galilean transformation. Thus we evaluate those in the center-of-mass frame of the entire simulated cluster.

### 2.2. *Comparison with Analysis Methods Adopted by Previous Work*

The set of basic equations that we adopt in this paper is essentially identical to that of Fang et al. (2009), except the fact that they interpreted the difference between $M_{\rm tot}$ and $M_{\rm therm} + M_{\rm rot} + M_{\rm stream}$ as "turbulent gas motion" while we call it the acceleration term $M_{\rm accel}$ as directly implied from equation (1), and evaluate it from the residual, $M_{\rm accel} = M_{\rm tot} - M_{\rm therm} - M_{\rm rot} - M_{\rm stream}$.

We are not sure why they ascribed the term to the turbulent motion. It is true that part of the gas acceleration would be due to the turbulent gas motion, but not entirely. Furthermore the numerical simulation does not include any physical processes directly related to the turbulent motion. Even if the turbulent motion might be important for real clusters, it should come from some physics below the subgrid scales that cannot be properly resolved in the numerical simulation. Effects of gas random motion above the resolved scales should be included in $M_{\rm rot}$ and $M_{\rm stream}$. We note, however, that the different interpretation of $M_{\rm accel}$ does not affect at all the conclusion of Fang et al. (2009) that gas rotation is the most important term to describe the origin of departure from HSE in their simulated clusters. As we will show below, this is not consistent with our result.

In previous literature, the Jeans equations are sometimes used in analyzing the gas motion in simulated clusters. For that purpose, a thermal pressure gradient term is added by hand to the basic equations (e.g., Rasia et al. 2004; Lau et al. 2009). Assuming the steady state, i.e., $\partial \boldsymbol{v}/\partial t = 0$, the Jeans equations in $r$-direction (A20) is now replaced by the following equation:

$$\begin{aligned} \left[ v_r \frac{\partial}{\partial r} + \frac{v_\theta}{r}\frac{\partial}{\partial \theta} + \frac{v_\varphi}{r\sin\theta}\frac{\partial}{\partial\varphi} \right] v_r + \frac{1}{\rho_{\rm gas}} \left[ \frac{1}{r}\frac{\partial(\rho_{\rm gas}\sigma^2_{r\theta})}{\partial\theta} + \frac{1}{r\sin\theta}\frac{\partial(\rho_{\rm gas}\sigma^2_{r\varphi})}{\partial\varphi} \right] + \frac{\sigma^2_{r\theta}\cot\theta}{r} \\ - \frac{v_\theta^2 + v_\varphi^2}{r} = -\frac{1}{\rho_{\rm gas}}\frac{\partial(\rho_{\rm gas}\sigma^2_{rr})}{\partial r} - \frac{2\sigma^2_{rr} - \sigma^2_{\theta\theta} - \sigma^2_{\varphi\varphi}}{r} - \frac{1}{\rho_{\rm gas}}\frac{\partial p}{\partial r} - \frac{\partial\phi}{\partial r}, \end{aligned} \tag{9}$$

where $\sigma^2_{ij}$ denotes the $ij$-component of the velocity dispersion tensor.

For example, Lau et al. (2009) converted each term of equation (9) to the corresponding mass term; see their equations (6) to (11). Then they interpreted that the first two terms on the right hand side of the above equation originate from "random gas motion". We suspect that the implicit assumption underlying equation (9) is that the ICM consists of two distinct gas components; the thermal gas and the unthermalized one such as the cold gas accreting along with galaxies into clusters. While it may be reasonable to take into account both components separately when dealing with *real galaxy clusters*, it remains to be justified if the extra pressure gradient term can be added by hand to the conventional Jeans equations assuming that the two components share the same density $\rho_{\rm gas}$ (In Appendix A we show that diagonal components of the velocity dispersion tensor in the Jeans equations correspond to thermal pressure in the Euler equations). It should also be recalled that the current numerical simulations are performed entirely on the basis of the Euler equations. Therefore, for the sake of consistency, it is appropriate to use the Euler equations, instead of equation (9), in evaluating the mass terms of the *simulated galaxy clusters*. The proper treatment of the unthermalized gas in numerical simulations is certainly an important issue, but is beyond the scope of the present paper.

## 3. APPLICATION TO A SIMULATED CLUSTER

We apply the analysis method in the previous section and quantitatively examine the validity of the HSE assumption. For that purpose, we use a simulated cluster of Cen (2012). It is simulated with an Eulerian adaptive mesh refinement (AMR) code, Enzo (Bryan 1999; Bryan & Norman 1999; O'Shea et al. 2004; Joung et al. 2009). Although our current analysis exploits three-dimensional profiles of the cluster which cannot be observed in reality, we are interested here in the validity of HSE itself. The application to the X-ray observation will be discussed separately elsewhere.

### 3.1. *Hydrodynamical Simulation*

We briefly describe the main features of the current simulation, and refer readers to Cen (2012) for more detail. The simulation was run first with a low resolution mode in a periodic box of 120 $h^{-1}$ Mpc on a side. Then a region centered on a cluster with a mass of $\sim 2\times10^{14}h^{-1}M_\odot$ was resimulated with a higher resolution in an adaptively refined manner. The size of the refined region is $21\times24\times20(h^{-1}\mathrm{Mpc})^3$. The mean interparticle separation and the dark matter particle mass in the refined region are 117 $h^{-1}$ kpc comoving and $1.07\times10^8h^{-1}M_\odot$, respectively.

Star particles are created according to the prescription of Cen & Ostriker (1992). Their typical mass is $\sim 10^6M_\odot$. The simulation includes a metagalactic UV background (Haardt & Madau 1996), shielding of UV radiation by neutral hydrogen (Cen et al. 2005) and metallicity-dependent radiative cooling (Cen et al. 1995). While supernova feedback is modeled following Cen et al. (2005), AGN feedback is not included in this simulation. The cosmological parameters used in this simulation are $(\Omega_b,\Omega_m,\Omega_\Lambda,h,n_s,\sigma_8) = (0.046,\ 0.28,\ 0.72,\ 0.70,\ 0.96,\ 0.82)$, following the WMAP7-normalized ΛCDM model (Komatsu et al. 2011).

Then a cluster is identified and the cubic box of a side of $3.8h^{-1}$ Mpc surrounding the entire cluster is extracted from the simulation data. The dark matter and stars are represented by particles, and the temperature and density of gas are given on the $520^3$ grids (the grid length is $7.324h^{-1}$kpc).

The radius $r_{500}$ of the cluster is $\sim 640h^{-1}$ kpc ($r_{500}$ is defined so that the mean density inside $r_{500}$ is 500 times the critical density of the universe). The center-of-mass velocity of the cluster within $r_{500}$ is set to vanish. The total mass $M_{500}$ within $r_{500}$ is $\sim 2\times10^{14}M_\odot$. The average ICM temperature at $r_{500}$ is $\sim 2$ keV, and the circular speed there is $v_{500}=\sqrt{GM_{500}/r_{500}}\sim 1000$ km s$^{-1}$.

Projected surface densities of gas, dark matter and stars on $x$-$z$ plane are plotted in the left panels of Figure 1. The right panels of Figure 1 show the three-dimensional view of the three components. The left (right) plots are color-coded according to the surface (space) densities normalized by the fraction of each component averaged over the box, $\tilde{\Omega}_k$ ($k=$ gas, dark matter and stars). Note that the fraction $\tilde{\Omega}_k$ is different from the density parameter $\Omega_k$ because the box is selected preferentially around the cluster.

As is clear from Figure 1, the gas distribution is smoother but very well traces the underlying dark matter distribution. In contract, stars are more significantly concentrated in high density regions, and exhibit numerous small clumps, most of which are not identified/resolved in the gas distribution.

Figure 2 plots the radial density and mass profiles of the cluster. The stellar fraction in the inner region ($r < 200h^{-1}$kpc) is significantly higher than the typical observed value. This is a well-known common problem among current high-resolution cosmological simulations, and implies that some important baryon physics including high-energy phenomena and star formation is still missing in the simulation. We perform the analysis of cluster gas, *assuming* that this excessive star densities in the inner region does not affect our conclusions at outer radius.

Figure 3 represents velocity fields in $x$-$y$, $y$-$z$ and $z$-$x$ planes passing through the center of the cluster. The red/blue arrows have negative/positive radial velocity, showing that the gas in the outer regions ($r\gtrsim 1h^{-1}$ Mpc) falls toward the center while its direction is randomized in the inner region.

### 3.2. *Results*

We evaluate the *effective* mass terms defined in Section 2 for the simulated cluster, which is plotted in Figure 5; the left panel shows the mass profiles, while the right panel indicates their fractional contribution to the total mass within the radius.

The total mass $M_{\rm tot}(r)$ is computed by directly summing up all the dark matter and star particles and gas of grids within the sphere of $r$. The other terms, $M_{\rm therm}$, $M_{\rm rot}$ and $M_{\rm stream}$, require the pressure and velocity fields evaluated at $r$. For that purpose, we use the density, velocity and temperature of gas defined at $520^3$ original grid points, and first bin the cluster into 50 logarithmically equal radial intervals between 90–1900 $h^{-1}$ kpc, $10\times10$ linearly equal angular intervals.

Integrands of equations (5), (6) and (7) are calculated in each bin. Derivatives of the physical variables such as $\partial p/\partial r$ are calculated as follows; first $\partial/\partial x$, $\partial/\partial y$ and $\partial/\partial z$ are computed from the difference of the adjacent the original Cartesian grid points. Then $\partial/\partial r$, $\partial/\partial\theta$ and $\partial/\partial\varphi$ in our spherical coordinates are calculated applying the chain rule.

In this way, $M_{\rm therm}(r)$, $M_{\rm rot}(r)$ and $M_{\rm stream}(r)$ are computed by integrating the corresponding integrands evaluated above. Finally we estimate $M_{\rm accel}$ simply from the residual of $M_{\rm accel}=M_{\rm tot}-M_{\rm therm}-M_{\rm rot}-M_{\rm stream}$, since we have the cluster data at $z=0$ alone. This estimate for $M_{\rm accel}$ may be different from the original defintion, i.e., equation (8). Indeed when we attempted to compute $M_{\rm accel}$ directly from the box mentioned in Section 3, it turned out to be too small to obtain a correct gravitational potential for the entire cluster. Thus we go back to a larger simulation box of a side of 22.5 $h^{-1}$ Mpc and the grid length of 29.34 $h^{-1}$ kpc that encloses our cluster. Then we compute the gravitational potential using FFT to obtain the gas acceleration at each grid point. This enables us to directly calculate $M_{\rm accel}$. Figure 4 is a comparison of $M_{\rm accel}$'s calculated by two methods. The directly calculated $M_{\rm accel}$ (magenta line) is in good agreement with $M_{\rm tot}-M_{\rm therm}-M_{\rm rot}-M_{\rm stream}$ (black line), although there is a large difference between the two within $200h^{-1}$ kpc. Also, we make sure that the sum $M_{\rm therm}+M_{\rm rot}+M_{\rm stream}+M_{\rm accel}$ reproduces $M_{\rm tot}$ within $\sim 2$ % except for the innermost region ($r < 200h^{-1}$ kpc), where it deviates from $M_{\rm tot}$ by up to $\sim 9$ %. Thus the estimation of $M_{\rm accel}$ by $M_{\rm tot}-M_{\rm therm}-M_{\rm rot}-M_{\rm stream}$ is sufficiently good given the quoted errors of our conclusion below. Although it seems better to use $M_{\rm accel}$ directly calculated from equation (8), the grid size of the larger box is so coarse that we cannot take advantage of the high resolution of the simulations in this study. Therefore, we decided to use the smaller box explained in Section 3 and $M_{\rm accel}$ is calculated by $M_{\rm tot}-M_{\rm therm}-M_{\rm rot}-M_{\rm stream}$ in the following analysis.

The left panel of Figure 5 implies that $M_{\rm therm}$ agrees with $M_{\rm tot}$ reasonably well. Each of the other three terms contributes less than 10 % of the total mass (the dotted curves correspond to the case in which each term becomes negative and its absolute value is plotted instead).

In order to consider the validity of HSE more quantitatively, we plot the fractional contribution of each mass term in the right panel of Figure 5. The rotation term, $M_{\rm rot}$, is always positive (by definition) and contributes approximately 10 % almost independently of radius. In contrast, the streaming velocity term, $M_{\rm stream}$, is mostly negative, and varies a lot at different radial bins. As a result, the difference of the total mass $M_{\rm tot}$ and the HSE mass $M_{\rm therm}$ is mostly explained by the acceleration term $M_{\rm accel}$ alone; compare the black and magenta curves in the right panel of Figure 5. At $r = r_{500}$ and $r_{200}$, the deviation from HSE in terms of the mass difference $(M_{\rm therm} - M_{\rm tot})/M_{\rm tot}$ is about 10 %. Nevertheless the value significantly varies at different radii and it is safe to conclude that $(M_{\rm therm} - M_{\rm tot})/M_{\rm tot}$ ranges approximately 10-20 % at $r < r_{200}$. Also there is no systematic trend of the validity of the HSE assumption as a function of radius. Even though the reliability of the simulation is suspicious for $r < 200h^{-1}$kpc due to the excessive stellar concentration (Section 3.1), $(M_{\rm therm} - M_{\rm tot})/M_{\rm tot}$ fluctuates between $-10$ % and $+25$ % for $300h^{-1}\mathrm{kpc} < r < r_{500}$. Thus there is no guarantee that HSE becomes a better approximation toward the inner central region.

Physically speaking, $M_{\rm rot} + M_{\rm stream} + M_{\rm accel} (= M_{\rm tot} - M_{\rm therm})$ corresponds to the term intergrating the Lagrangian derivative of the gas velocity over the sphere. Therefore the fact that it is small compared with $M_{\rm therm}$ and $M_{\rm tot}$ is simply translated into the condition of HSE that the gas acceleration from a Lagrangian point of view is negligible compared with the pressure gradient and the total gravity.

Since we analyze a single simulated cluster, it is not clear to what extent our interpretation that $M_{\rm accel}$ determines the departure from HSE holds in general. Thus we use a different set of SPH simulation clusters (Dolag et al. 2009) kindly provided by Klaus Dolag. For these clusters, we assume spherical symmetry and do not divide the spherical surface at a given radius just for simplicity. Klaus Dolag also provides us with $M_{\rm accel}$ directly computed from the acceleration data. We find that in most cases $|M_{\rm accel}|$ is larger than $M_{\rm rot}$ and $|M_{\rm stream}|$ especially where $M_{\rm therm}$ deviates from $M_{\rm tot}$. We also confirm that $M_{\rm therm} + M_{\rm rot} + M_{\rm stream} + M_{\rm accel}$ reproduces $M_{\rm tot}$ within $\sim 5$ % for most regions (See Appendix C).

The above results basically support our conclusion for the cluster from the AMR simulations, but we do not have a statistical discussion including clusters from the SPH simulations because of the differences in resolutions and simulation methods. Instead, we divide the AMR cluster into two regions; upper and lower hemispheres with respect to the *x*-*y* plane. Then we duplicate each hemisphere into one cluster. We call the synthetic cluster constructed from the $z > 0$ ($z < 0$) hemisphere "z+" ("z-"). Although these clusters are of course not independent of the original cluster and we cannot make a statistical argument on their properties, we can briefly look at the effects of substructures or inhomogeneity of temperature and velocity field.

We repeat the same analysis on these two synthetic clusters, and the results are plotted in Figure 6. The amplitudes of the different terms vary significantly between the two clusters, and the degree of the validity of HSE is also very different. Nevertheless the generic trend is clear; the relation of $M_{\rm accel} \approx M_{\rm tot} - M_{\rm therm}$ holds almost independently of $r$.

It is not clear, however, why the two hemispheres have so different values of $(M_{\rm tot} - M_{\rm therm})/M_{\rm tot}$; HSE holds very well for "z+", while it is not the case for "z-". The visual inspection of Figure 1 does not reveal any significant difference between the two. It may be because some local concentrations of dark matter enhance the acceleration/deceleration of gas, and influence the overall non-sphericity of the gas density. Thus the analysis taking account of the ellipticity may provide a deeper insight on the validity of HSE, but is beyond the scope of the present paper.

## 4. CONCLUSION

We have examined the validity of HSE that has been conventionally assumed in estimating the mass of galaxy clusters from X-ray observations. We use a simulated cluster and evaluate several mass terms directly corresponding to the Euler equations that govern the gas dynamics. We find that the mass estimated under the HSE assumption, $M_{\rm therm}$ in the present study, deviates from the true mass $M_{\rm tot}$ on average by $\sim (10 - 20)$ % fractionally for $r < r_{200}$. There is no clear tendency that the HSE becomes a better approximation toward the inner region. More importantly, we find that $M_{\rm tot} - M_{\rm therm}$ is nearly identical to $M_{\rm accel}$, in other words, the validity of HSE is controlled by the amount of gas acceleration. This trend is confirmed by the separate analysis of the different hemispheres of the same simulated cluster.

Our current analysis is limited to a single simulated cluster, but the overall conclusion that the HSE mass agrees with the total mass within (10-20)% is consistent with previous results by Fang et al. (2009) and Lau et al. (2009). Nevertheless the interpretation of the origin of the departure from HSE is very different. Fang et al. (2009) concluded that the gas rotation term $M_{\rm rot}$ makes a significant contribution and that $M_{\rm therm} + M_{\rm rot}$ well reproduces the total mass, especially for relaxed clusters. It is not the case, however, for our simulated cluster at least. Similarly Lau et al. (2009) found the similar degree of the departure from HSE, but they ascribed the discrepancy to the random gas motion. Their analysis, however, is based on the modification of the Jeans equations, which does not appear to be justified for the analysis of the gas dynamics, and thus their conclusion should be interpreted with caution.

A relatively small systematic error of the HSE mass inferred from current numerical simulations may be partly ascribed to the assumptions inherent in the Euler equations, i.e., local thermal equilibrium and negligible viscosity (Appendix A). This is supported by the fact that the error in the mass estimated from the random motion of collisionless particles tends to be much greater at large radii (Appendix B) because the relaxation time scale for collisionless particles are appreciably longer than that for collisional gas. We should also note that the HSE mass can be influenced by other physical precesses that are not included in the numerical simulations, such as pressure support from micro-turbulence, the magnetic field, and accelerated particles (e.g., Laganá et al. 2010). The neglected components mentioned above are closely linked with one another (e.g., viscosity can play a role in generating turbulence and the magnetic field can affect both thermalization and acceleration of gas particles) and will be investigated in the near future by X-ray missions such as NuSTAR[10] and ASTRO-H as well as by radio telescopes including EVLA[11] and LOFAR[12].

The present analysis is fairly idealized in a sense that the evaluation of all the mass terms has been done from the full three dimensional data of simulated clusters. In reality observational data of X-ray clusters are basically projected along the line of sight. Therefore additional uncertainties and systematic errors may become important as well. Also it is necessary to carry out the current analysis for a number of clusters in order to obtain the statistically robust conclusion. These issues will be discussed elsewhere.

## ACKNOWLEDGMENTS

We thank an anonymous referee for useful comments, in particular on the role of the unthermalized gas component as discussed in Section 2.2. We also thank Klaus Dolag for kindly providing us with SPH simulation data and calculating the gas acceleration, and Fujihiro Hamba for a useful comment on the interpretation of the inertial term in the Euler equations. Y.S. gratefully acknowledges support from the Global Scholars Program of Princeton University. This work is supported in part by the Grants-in-Aid for Scientific Research by the Japan Society for the Promotion of Science (JSPS) (PD:22-5467, 21740139, 20340041, 24340035) and JSPS Core-to-Core Program “International Research Network for Dark Energy”. Computing resources were in part provided by the NASA High-End Computing (HEC) Program through the NASA Advanced Supercomputing (NAS) Division at Ames Research Center. The work of R.C. is supported in part by grants NNX11AI23G.

## REFERENCES

Allen, S. W., Evrard, A. E. & Mantz, A. B. 2011, MNRAS, 49, 409
Biffi, V., Dolag, K. & Böhringer, H. 2011, MNRAS, 413, 573
Bryan, G. L. 1999, Comput. Sci. Eng., 1, 46
Bryan, G. L., Norman, M. L., 1999, in Structured Adaptive Mesh Refinement Grid Methods, ed. N. P. C. S. B. Baden (IMA Volumes on Structured Adaptive Mesh Refinement Methods, No. 117), 165
Cen, R., & Ostriker, J. P. 1992, ApJ, 399, L113
Cen, R., Kang, H., Ostriker, J. P. & Ryu, D. 1995, ApJ, 451, 436
Cen, R., Nagamine, K. & Ostriker, J. P. 2005, ApJ, 635, 86
Cen, R. 2012, ApJ, 748, 121
Chapman, S. & Cowling, T. G., 1970, The Mathematical Theory of Non-Uniform Gases (3rd ed.; Cambridge, UK: Cambridge University Press)
Choudhuri, A., R., 1998, The Physics of Fluids and Plasmas: An Introduction for Astrophysics (Cambridge, UK: Cambridge University Press)
Dolag, K., Borgani, S., Murante, G. & Springel, V. 2009, MNRAS, 399, 497
Fang, T., Humphrey, P. & Buote, D. 2009, ApJ, 691, 1648
Haardt, F., & Madau, P. 1996, ApJ, 461, 20
Joung, M. R., Cen, R. & Bryan, G. L. 2009, ApJ, 692, L1
Komatsu E., Smith, K. M., Dunkley, J. et al., 2011, ApJS, 192, 18
Laganá, T. F., de Souza, R. S. & Keller, G. R. 2010, A&A 510, A76
Lau, E., Kravtsov, A. V. & Nagai, D. 2009, ApJ, 705, 1129
Mahdavi, A., Hoekstra, H., Babul, A. & Henry, P. 2008, MNRAS, 384, 1567
Nagai, D., Vikhlinin, A., & Kravtsov, A. V. 2007, ApJ, 655, 98
O'Shea, B. W., Bryan, G., Bordner et al., 2004, arXiv: 0403044
Rasia E., Tormen, G. & Moscardini, L. 2004, MNRAS, 351, 237
Zhang, Y.-Y., Finoguenov, A., Böhringer, H. et al. 2008, A&A, 482, 451

---

[10] http://www.nustar.caltech.edu
[11] http://www.aoc.nrao.edu/evla
[12] http://www.lofar.org

## APPENDIX

## RELATION BETWEEN THE EULER EQUATIONS AND THE JEANS EQUATIONS

From a microscopic point of view, both the Euler equations and the Jeans equations can be derived from the Boltzmann equation under different assumptions. In the following, we explicitly compare the two sets of equations in both Cartesian and spherical coordinates.

### *Cartesian Coordinates*

We define the distribution function $f$ such that $f(\boldsymbol{x}, \boldsymbol{v}, t) d^3x d^3v$ is the probability that a randomly chosen particle in the system lies in the phase space volume $d^3x d^3v$ at position $(\boldsymbol{x}, \boldsymbol{v})$ and time $t$. The motion of such particles under the gravitational potential $\phi$ is described by the Boltzmann equation:

$$\frac{\partial f}{\partial t} + v^i \frac{\partial f}{\partial x^i} - \frac{\partial \phi}{\partial x_i} \frac{\partial f}{\partial v^i} = \left( \frac{\delta f}{\delta t} \right)_{\rm coll}, \tag{A1}$$

where the collision term on the right hand side takes account of collisions between particles. Note that $v^i$ $(i = 1, 2, 3)$ represents a coordinate in the phase space and should not be confused with the velocity field at the spatial point $x^i$. For simplicity, we assume that all particles have the same mass $m$ in the following.

First, we consider a collisionless case with $(\delta f/\delta t)_{\rm coll} = 0$. Multiplying equation (A1) by $m$ and integrating it over the velocity space yield the continuity equation:

$$\frac{\partial \rho}{\partial t} + \frac{\partial(\rho \bar{v}^i)}{\partial x^i} = 0, \tag{A2}$$

where

$$\rho(\boldsymbol{x}, t) = \int d^3v \; mf(\boldsymbol{x}, \boldsymbol{v}, t) \tag{A3}$$

and we introduce the average over the velocity space:

$$\bar{q}(\boldsymbol{x}, t) = \frac{1}{\rho(\boldsymbol{x}, t)} \int d^3v \; mq(\boldsymbol{x}, \boldsymbol{v}, t) f(\boldsymbol{x}, \boldsymbol{v}, t) \tag{A4}$$

for an arbitrary variable $q$ such as $v^i$. Multiplying equation (A1) by $mv^j$ and integrating over the velocity space give the momentum equations:

$$\frac{\partial(\rho \bar{v}^i)}{\partial t} + \frac{\partial \tau_{\rm J}^{ij}}{\partial x^j} = -\rho \frac{\partial \phi}{\partial x_i}, \tag{A5}$$

where

$$\tau_{\rm J}^{ij} = \rho \overline{v^i v^j} = \rho \sigma^{2,ij} + \rho \bar{v}^i \bar{v}^j \tag{A6}$$

and $\sigma^{2,ij}$ is the velocity dispersion tensor. Equations (A2) and (A5) reduce to the Jeans equations:

$$\frac{\partial \bar{v}^i}{\partial t} + \bar{v}^j \frac{\partial \bar{v}^i}{\partial x^j} = -\frac{1}{\rho} \frac{\partial(\rho \sigma^{2,ij})}{\partial x^j} - \frac{\partial \phi}{\partial x_i} \tag{A7}$$

Next, we consider a collisional case. Rigorous handling of the collisional term is rather complicated and simplified models are often used. A conventional one is the Bhartnagar-Gross-Krock (BGK) equation, which employs a linearized collisional term:

$$\frac{\partial f}{\partial t} + v^i \frac{\partial f}{\partial x^i} - \frac{\partial \phi}{\partial x_i} \frac{\partial f}{\partial v^i} = -\frac{f - f_0}{\tau}, \tag{A8}$$

where $\tau$ is the relaxation time of the system considered, $f_0$ is the Maxwellian distribution function characterized by the local temperature $T(\boldsymbol{x}, t)$:

$$f_0(\boldsymbol{x}, \boldsymbol{v}, t) = \left[\frac{m}{2\pi k_B T(\boldsymbol{x}, t)}\right]^{3/2} \exp\left[-\frac{m(\boldsymbol{v} - \bar{\boldsymbol{v}}(\boldsymbol{x}, t))^2}{2k_B T(\boldsymbol{x}, t)}\right], \tag{A9}$$

and $k_B$ is the Boltzmann constant. If we assume that mean values of conservatives such as mass and momentum are the same as those in local thermal equilibrium, the collision term vanishes in the continuity and momentum equations. In local thermal equilibrium, pressure is defined from the diagonal components of $\sigma_{ij}^2$ by $p\delta_{ij} \equiv \rho \sigma_{ij}^2$ and the dispersion tensor can be written as

$$\tau_{\rm E}^{ij} = p\delta^{ij} + \rho \bar{v}^i \bar{v}^j. \tag{A10}$$

If we replace $\tau_{\rm J}$ in equation (A5) with $\tau_{\rm E}$ and combine them with equation (A2), we obtain the Euler equations:

$$\frac{\partial \bar{v}^i}{\partial t} + \bar{v}^j \frac{\partial \bar{v}^i}{\partial x^j} = -\frac{1}{\rho} \frac{\partial p}{\partial x_i} - \frac{\partial \phi}{\partial x_i}. \tag{A11}$$

The difference between the Euler and the Jeans equations resides only in the form of the dispersion tensor.

If we retain the off-diagonal components of the dispersion tensor, they can be interpreted as viscosity, and the equations reduce to the Navier-Stokes equations (Choudhuri 1998; Chapman & Cowling 1970).

### *Spherical coordinates*

One can rewrite the continuity and momentum equations in the previous section in general coordinates:

$$\frac{\partial \rho}{\partial t} + \nabla_i (\rho \bar{v}^i) = 0 \tag{A12}$$

and

$$\frac{\partial(\rho \bar{v}^i)}{\partial t} + \nabla_j \tau^{ij} = -\rho g^{ij} \nabla_j \phi, \tag{A13}$$

by using the *covariant* derivative operator $\nabla_i$ . For spherical coordinates $(x^1 = r, x^2 = \theta, x^3 = \varphi)$, non-zero components of the metric tensor $g^{ij}$ are

$$g_{11} = 1, \quad g_{22} = r^2, \quad g_{33} = r^2 \sin^2 \theta \tag{A14}$$

and the corresponding non-zero connection coefficients are

$$\begin{aligned}
&\Gamma^1_{22} = -r, \quad \Gamma^1_{33} = -r\sin^2\theta, \quad \Gamma^2_{12} = \Gamma^2_{21} = \frac{1}{r},\\
&\Gamma^2_{33} = -\sin\theta\cos\theta, \quad \Gamma^3_{13} = \Gamma^3_{31} = \frac{1}{r}, \quad \Gamma^3_{23} = \Gamma^3_{32} = \cot\theta.
\end{aligned} \tag{A15}$$

The velocity vector is now given by $\bar{v}^i = (\bar{v}_r, \bar{v}_\theta/r, \bar{v}_\varphi/r\sin\theta)$.

In spherical coordinates, the continuity equation reads

$$\frac{\partial\rho}{\partial t} + \frac{1}{r^2}\frac{\partial(r^2\rho\bar{v}_r)}{\partial r} + \frac{1}{r\sin\theta}\frac{\partial(\sin\theta\rho\bar{v}_\theta)}{\partial\theta} + \frac{1}{r\sin\theta}\frac{\partial(\rho\bar{v}_\varphi)}{\partial\varphi} = 0. \tag{A16}$$

Setting $\tau^{ij} = \tau^{ij}_{\rm E} = \rho\bar{v}^i\bar{v}^j + pg^{ij}$ gives the Euler equations:

$$\left[\frac{\partial}{\partial t} + \bar{v}_r\frac{\partial}{\partial r} + \frac{\bar{v}_\theta}{r}\frac{\partial}{\partial\theta} + \frac{\bar{v}_\varphi}{r\sin\theta}\frac{\partial}{\partial\varphi}\right]\bar{v}_r - \frac{\bar{v}_\theta^2 + \bar{v}_\varphi^2}{r} = -\frac{1}{\rho}\frac{\partial p}{\partial r} - \frac{\partial\phi}{\partial r} \tag{A17}$$

$$\left[\frac{\partial}{\partial t} + \bar{v}_r\frac{\partial}{\partial r} + \frac{\bar{v}_\theta}{r}\frac{\partial}{\partial\theta} + \frac{\bar{v}_\varphi}{r\sin\theta}\frac{\partial}{\partial\varphi}\right]\bar{v}_\theta + \frac{\bar{v}_r\bar{v}_\theta - \bar{v}_\varphi^2\cot\theta}{r} = -\frac{1}{\rho r}\frac{\partial p}{\partial\theta} - \frac{1}{r}\frac{\partial\phi}{\partial\theta} \tag{A18}$$

$$\left[\frac{\partial}{\partial t} + \bar{v}_r\frac{\partial}{\partial r} + \frac{\bar{v}_\theta}{r}\frac{\partial}{\partial\theta} + \frac{\bar{v}_\varphi}{r\sin\theta}\frac{\partial}{\partial\varphi}\right]\bar{v}_\varphi + \frac{\bar{v}_r\bar{v}_\varphi + \bar{v}_\theta\bar{v}_\varphi\cot\theta}{r} = -\frac{1}{\rho r\sin\theta}\frac{\partial p}{\partial\varphi} - \frac{1}{r\sin\theta}\frac{\partial\phi}{\partial\varphi}. \tag{A19}$$

On the other hand, putting $\tau^{ij} = \tau^{ij}_{\rm J} = \rho\overline{v^iv^j}$ leads to the Jeans equations

$$\begin{aligned}
&\left[\frac{\partial}{\partial t} + \bar{v}_r\frac{\partial}{\partial r} + \frac{\bar{v}_\theta}{r}\frac{\partial}{\partial\theta} + \frac{\bar{v}_\varphi}{r\sin\theta}\frac{\partial}{\partial\varphi}\right]\bar{v}_r + \frac{1}{\rho}\left[\frac{\partial(\rho\sigma^2_{rr})}{\partial r} + \frac{1}{r}\frac{\partial(\rho\sigma^2_{r\theta})}{\partial\theta} + \frac{1}{r\sin\theta}\frac{\partial(\rho\sigma^2_{r\varphi})}{\partial\varphi}\right]\\
&+ \frac{1}{r}\left(2\sigma^2_{rr} - \sigma^2_{\theta\theta} - \sigma^2_{\varphi\varphi} - \bar{v}_\theta^2 - \bar{v}_\varphi^2 + \sigma^2_{r\theta}\cot\theta\right) = -\frac{\partial\phi}{\partial r}
\end{aligned} \tag{A20}$$

$$\begin{aligned}
&\left[\frac{\partial}{\partial t} + \bar{v}_r\frac{\partial}{\partial r} + \frac{\bar{v}_\theta}{r}\frac{\partial}{\partial\theta} + \frac{\bar{v}_\varphi}{r\sin\theta}\frac{\partial}{\partial\varphi}\right]\bar{v}_\theta + \frac{1}{\rho}\left[\frac{\partial(\rho\sigma^2_{r\theta})}{\partial r} + \frac{1}{r}\frac{\partial(\rho\sigma^2_{\theta\theta})}{\partial\theta} + \frac{1}{r\sin\theta}\frac{\partial(\rho\sigma^2_{\theta\varphi})}{\partial\varphi}\right]\\
&+ \frac{1}{r}\left(3\sigma^2_{r\theta} - \sigma^2_{\varphi\varphi}\cot\theta + \bar{v}_r\bar{v}_\theta - \bar{v}_\varphi^2\cot\theta + \sigma^2_{\theta\theta}\cot\theta\right) = -\frac{1}{r}\frac{\partial\phi}{\partial\theta}
\end{aligned} \tag{A21}$$

$$\begin{aligned}
&\left[\frac{\partial}{\partial t} + \bar{v}_r\frac{\partial}{\partial r} + \frac{\bar{v}_\theta}{r}\frac{\partial}{\partial\theta} + \frac{\bar{v}_\varphi}{r\sin\theta}\frac{\partial}{\partial\varphi}\right]\bar{v}_\varphi + \frac{1}{\rho}\left[\frac{\partial(\rho\sigma^2_{r\varphi})}{\partial r} + \frac{1}{r}\frac{\partial(\rho\sigma^2_{\theta\varphi})}{\partial\theta} + \frac{1}{r\sin\theta}\frac{\partial(\rho\sigma^2_{\varphi\varphi})}{\partial\varphi}\right]\\
&+ \frac{1}{r}\left(3\sigma^2_{r\varphi} + \bar{v}_r\bar{v}_\varphi + \bar{v}_\theta\bar{v}_\varphi\cot\theta + 2\sigma^2_{\theta\varphi}\cot\theta\right) = -\frac{1}{r\sin\theta}\frac{\partial\phi}{\partial\varphi}.
\end{aligned} \tag{A22}$$

## SYSTEMATIC ERRORS IN MASS ESTIMATES FOR COLLISIONLESS SYSTEMS

In a similar fashion to Section 2.1, we can compute the gravitational mass using the Jeans equations:

$$\frac{\partial\boldsymbol{v}}{\partial t} + (\boldsymbol{v}\cdot\nabla)\boldsymbol{v} = -\frac{1}{\rho_{\rm dm}}\nabla(\rho_{\rm dm}\boldsymbol{\sigma}^2) - \nabla\phi, \tag{B1}$$

$$M_{\rm tot} = \frac{1}{4\pi G}\int_{\partial V} d\boldsymbol{S}\cdot\left[-\frac{1}{\rho_{\rm dm}}\nabla(\rho_{\rm dm}\boldsymbol{\sigma}^2) - (\boldsymbol{v}\cdot\nabla)\boldsymbol{v} - \frac{\partial\boldsymbol{v}}{\partial t}\right], \tag{B2}$$

where $\boldsymbol{v}$ and $\boldsymbol{\sigma}^2$ are the velocity field of particles and the velocity dispersion tensor, respectively. We here represent the collisionless component by dark matter, but the same formulation is readily applicable to galaxies. We decompose the right hand side of equation (B2) into the following terms by means of equation (A20):

$$M_{\rm tot} = M_{\rm rand} + M_{\rm aniso} + M_{\rm rot} + M_{\rm stream} + M_{\rm cross} + M_{\rm accel}. \tag{B3}$$

$$M_{\rm rand} = -\frac{1}{4\pi G}\int_{\partial V} dS\ \frac{1}{\rho_{\rm dm}}\frac{\partial(\rho_{\rm dm}\sigma^2_{rr})}{\partial r}, \tag{B4}$$

$$M_{\rm aniso} = -\frac{1}{4\pi G}\int_{\partial V} dS\ \frac{2\sigma^2_{rr} - \sigma^2_{\theta\theta} - \sigma^2_{\varphi\varphi}}{r}, \tag{B5}$$

$$M_{\rm rot} = \frac{1}{4\pi G}\int_{\partial V} dS\ \frac{v_\theta^2 + v_\varphi^2}{r}, \tag{B6}$$

$$M_{\rm stream} = -\frac{1}{4\pi G}\int_{\partial V} dS\ \left[v_r\frac{\partial v_r}{\partial r} + \frac{v_\theta}{r}\frac{\partial v_r}{\partial \theta} + \frac{v_\varphi}{r\sin\theta}\frac{\partial v_r}{\partial\varphi}\right], \tag{B7}$$

$$M_{\rm cross} = -\frac{1}{4\pi G}\int_{\partial V} dS\ \left[\frac{1}{\rho_{\rm dm} r}\frac{\partial(\rho_{\rm dm}\sigma^2_{r\theta})}{\partial\theta} + \frac{1}{\rho_{\rm dm} r\sin\theta}\frac{\partial(\rho_{\rm dm}\sigma^2_{r\varphi})}{\partial\varphi} + \frac{\sigma^2_{r\theta}\cot\theta}{r}\right]. \tag{B8}$$

$$M_{\rm accel} = -\frac{1}{4\pi G}\int_{\partial V} dS\ \frac{\partial v_r}{\partial t}. \tag{B9}$$

Physical interpretation of each mass term is as follows. The term $M_{\rm rand}$ comes from the gradient of velocity dispersion in the $r$-direction and corresponds to $M_{\rm therm}$ for a collisional gas. The meaning of $M_{\rm rot}$, $M_{\rm stream}$ and $M_{\rm accel}$ are similar to the corresponding terms for the collisional gas (equations (6) to (8)). The terms that have no counterpart in the Euler equations are $M_{\rm aniso}$ and $M_{\rm cross}$; the former represents anisotropy of the velocity dispersion whereas the latter arises from the off-diagonal components of the velocity dispersion tenser and vanishes if velocities of different directions are uncorrelated.

We apply the above formulation to dark matter particles in the simulated cluster described in Section 3 to quantify intrinsic systematic errors of the mass estimation using collisionless particles. Note that one can apply the same method to galaxies but with much larger impact of statistical errors. Therefore, we do not do so here because we are interested in intrinsic systematic errors independent of observational complexities. Each term is computed in a similar manner to the case of collisional gas described in Section 3.

Figure 7 shows that the difference between $M_{\rm tot}$ and $M_{\rm rand}$ increases toward the outer envelope mainly owing to the presence of $M_{\rm aniso}$. This is because the relaxation timescale of collisionless particles is much longer than that of the collisional gas. Once this term is subtracted, $M_{\rm tot} - M_{\rm rand} - M_{\rm aniso}$ closely matches $M_{\rm accel}$ whose absolute value is limited to within $\sim 0.3M_{\rm tot}$. The amount of $M_{\rm accel}$ is similar to that for the collisional gas (Fig. 5). The other mass terms such as $M_{\rm cross}$ are less important.

The above results imply that proper account of velocity anisotropies is essential for the mass reconstruction using a collisionless component. We stress that $M_{\rm aniso}$ is irrelevant to the collisional fluid as long as local thermal equilibrium is established (Appendix A).

## VALIDITY OF HYDROSTATIC EQUILIBRIUM IN CLUSTERS FROM SMOOTHED PARTICLE HYDRODYNAMICS SIMULATION

We have shown the behavior of the mass terms for the cluster from the AMR simulation in Section 4. Especially, the HSE mass deviates from the total mass by up to $\sim 30$ % and the difference is explained chiefly by the gas acceleration. In order to make sure if such behavior is common to simulated clusters, we analyze the other simulated clusters. Since our AMR simulation includes only a single cluster, we analyze clusters extracted from a smoothed particle hydrodynamics (SPH) simulation performed by Dolag et al. (2009) using GADGET-2 to confirm the results in Section 4. We refer Dolag et al. (2009) for the detail of the simulation.

We use five regions named g1, g72, g1542, g3344 and g914 extracted from the simulation. Each region has a cluster near the center and the cluster is labeled “a” (g1a, g72a, g1542a, g3344a, g914a). For each cluster, we make $256^3$ mesh data centered on the cluster's center-of-mass within the radius $r_{500}$. The size of the data box is determined so that it contains the entire sphere of radius $3r_{500}$ centered on the cluster's center-of-mass.

We calculate the mass terms defined in Section 2 for the five simulated clusters. Since we have the gas acceleration data, we calculate $M_{\rm accel}$ directly from the data without using $M_{\rm tot} - M_{\rm therm} - M_{\rm rot} - M_{\rm stream}$.

Figure 8 shows the result for the cluster g914a. This figure basically supports the results in Section 4 in that $M_{\rm therm}$ deviates from $M_{\rm tot}$ by $\sim 30\%$ at most and that $M_{\rm accel}$ becomes large where the difference between $M_{\rm tot}$ and $M_{\rm therm}$ is large. The fact that the sum $M_{\rm therm} + M_{\rm rot} + M_{\rm stream} + M_{\rm accel}$ is approximately $M_{\rm tot}$ means the estimation of $M_{\rm accel}$ by $M_{\rm tot} - M_{\rm therm} - M_{\rm rot} - M_{\rm stream}$ is good, as confirmed in Section 4 for the AMR cluster.

Although not graphically shown, the mass terms for the other simulated clusters also exhibit similar behavior.

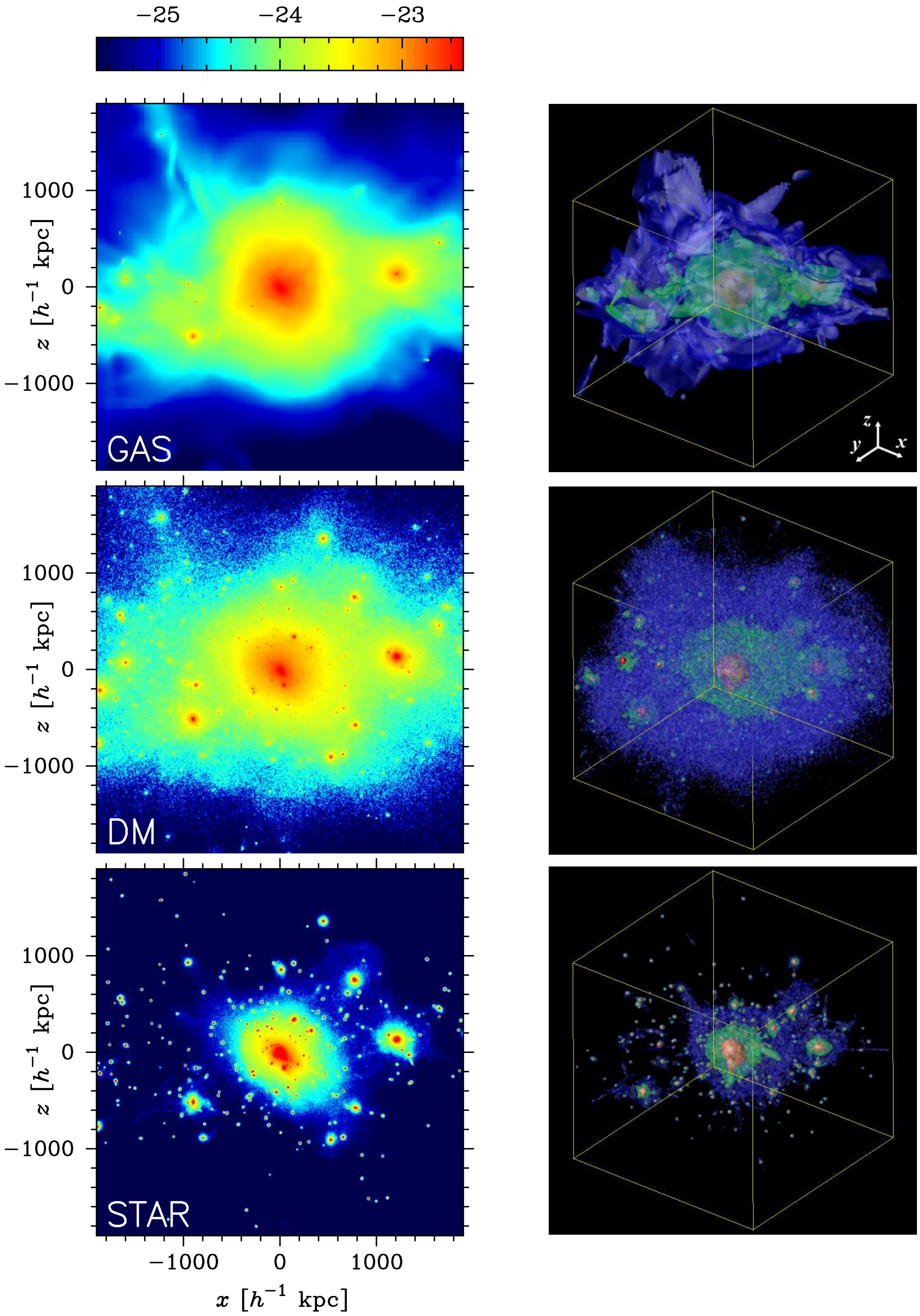

FIG. 1.— Densities of gas (top), dark matter (middle) and stars (bottom) are shown in two ways for each. *Left*: Projected surface densities on $x$-$z$ plane normalized by the fraction of each component in the box: $\log_{10}[\int dl\ \rho_k \tilde{\Omega}_k^{-1}\ /(\mathrm{g\ cm^{-3}}\ h^{-1}\ \mathrm{kpc})]$, where $k$ is one of gas, dark matter and stars and $\tilde{\Omega}_k$ is the fraction of $k$ component in the box. *Right*: Equal-density surfaces for $\log_{10}[\rho_k \tilde{\Omega}_k^{-1}/(\mathrm{g\ cm^{-3}}\ h^{-1}\ \mathrm{kpc})]=-28.0$ (blue), $-27.0$ (green) and $-26.0$ (red). Densities are normalized in the same way as the left panel.

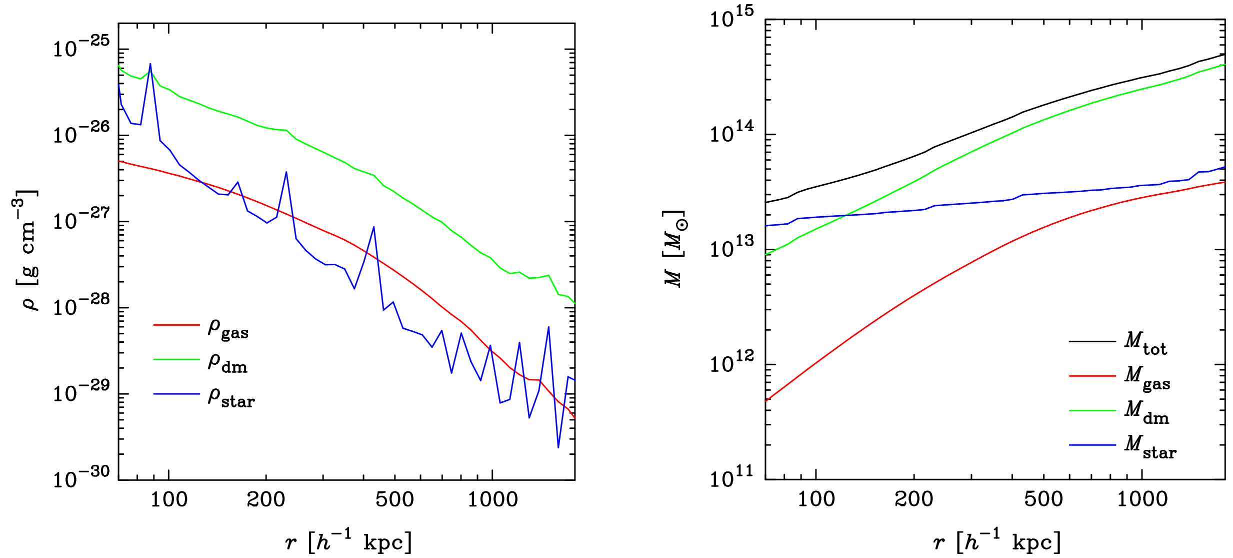

FIG. 2.— Radial profiles of densities (left) and masses (right) are shown for gas (red), dark matter (green) and stars (blue). The black line in the right panel shows the total gravitational mass; $M_{\text{tot}} = M_{\text{gas}} + M_{\text{dm}} + M_{\text{star}}$. The analysis is performed on the 50 logarithmically equal radial bins.

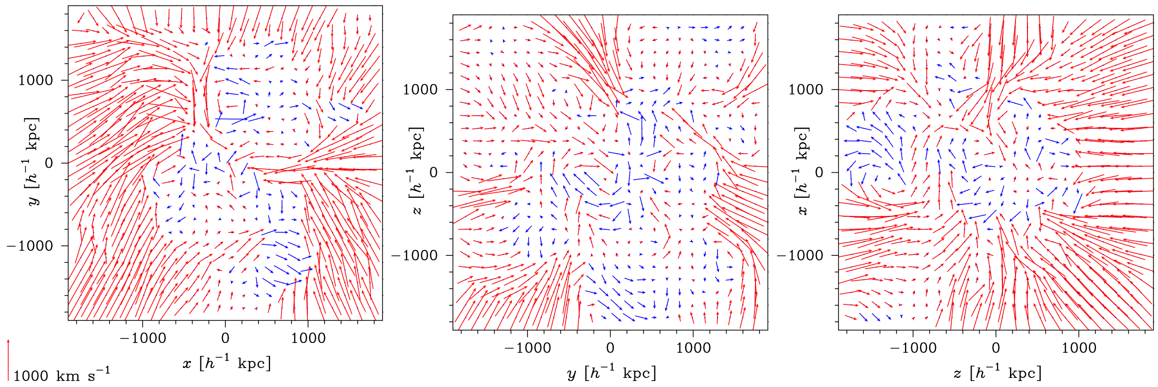

FIG. 3.— Velocity fields in $x$-$y$ (left), $y$-$z$ (middle) and $z$-$x$ (right) planes passing through the center of the cluster. The arrow is red if $v_r < 0$, and blue if $v_r > 0$. The length of the arrow is proportional to the magnitude of the velocity. An arrow with a speed of 1000 km s$^{-1}$ is shown for reference.

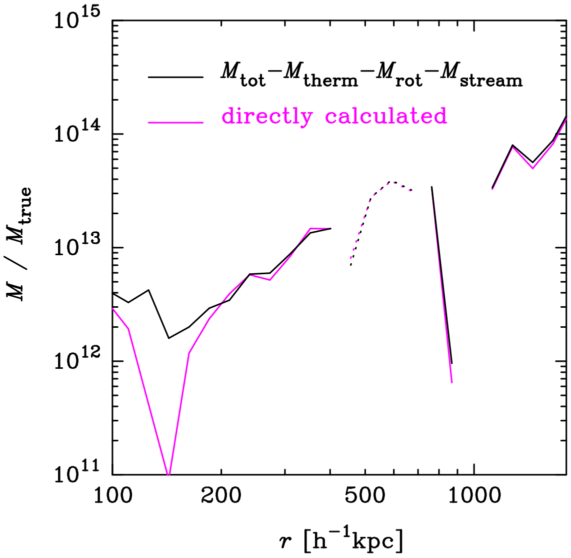

FIG. 4.— As comparison of the acceleration mass $M_{\rm accel}$ calculated directly from the acceleration data (magenta) and $M_{\rm tot} - M_{\rm therm} - M_{\rm rot} - M_{\rm stream}$ (black). Dotted line means that its sign is inverted. The analysis is performed on the 25 logarithmically equal radial bins.

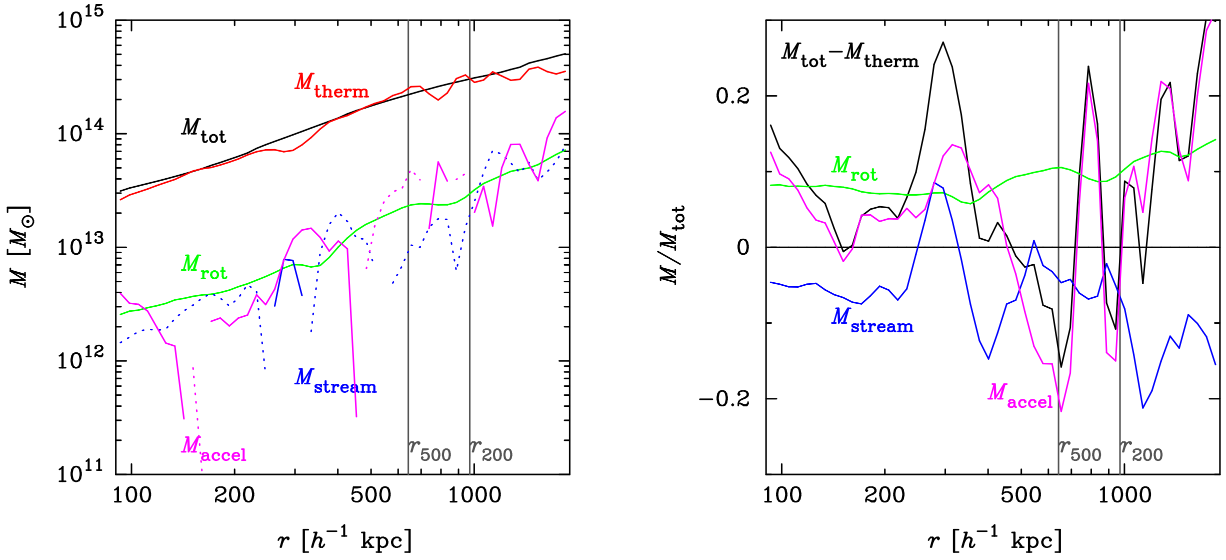

FIG. 5.— The *effective* mass terms in Equation (4) for the gas in the simulated cluster are shown in the left panel: $M_{\rm tot}$ (black), $M_{\rm therm}$ (red), $M_{\rm rot}$ (green), $M_{\rm stream}$ (blue) and $M_{\rm accel}$ (magenta). Here $M_{\rm accel}$ is calculated by $M_{\rm accel} = M_{\rm tot} - M_{\rm therm} - M_{\rm rot} - M_{\rm stream}$. Dotted line means that its sign is inverted. Ratios of mass terms to $M_{\rm tot}$ are shown in the right panel. The black line shows $(M_{\rm tot} - M_{\rm therm})/M_{\rm tot}$ and colored lines represent the same things as the left panel. The analysis is performed on the 50 logarithmically equal radial bins and 10 linearly equal bins both in polar and azimuthal angles.

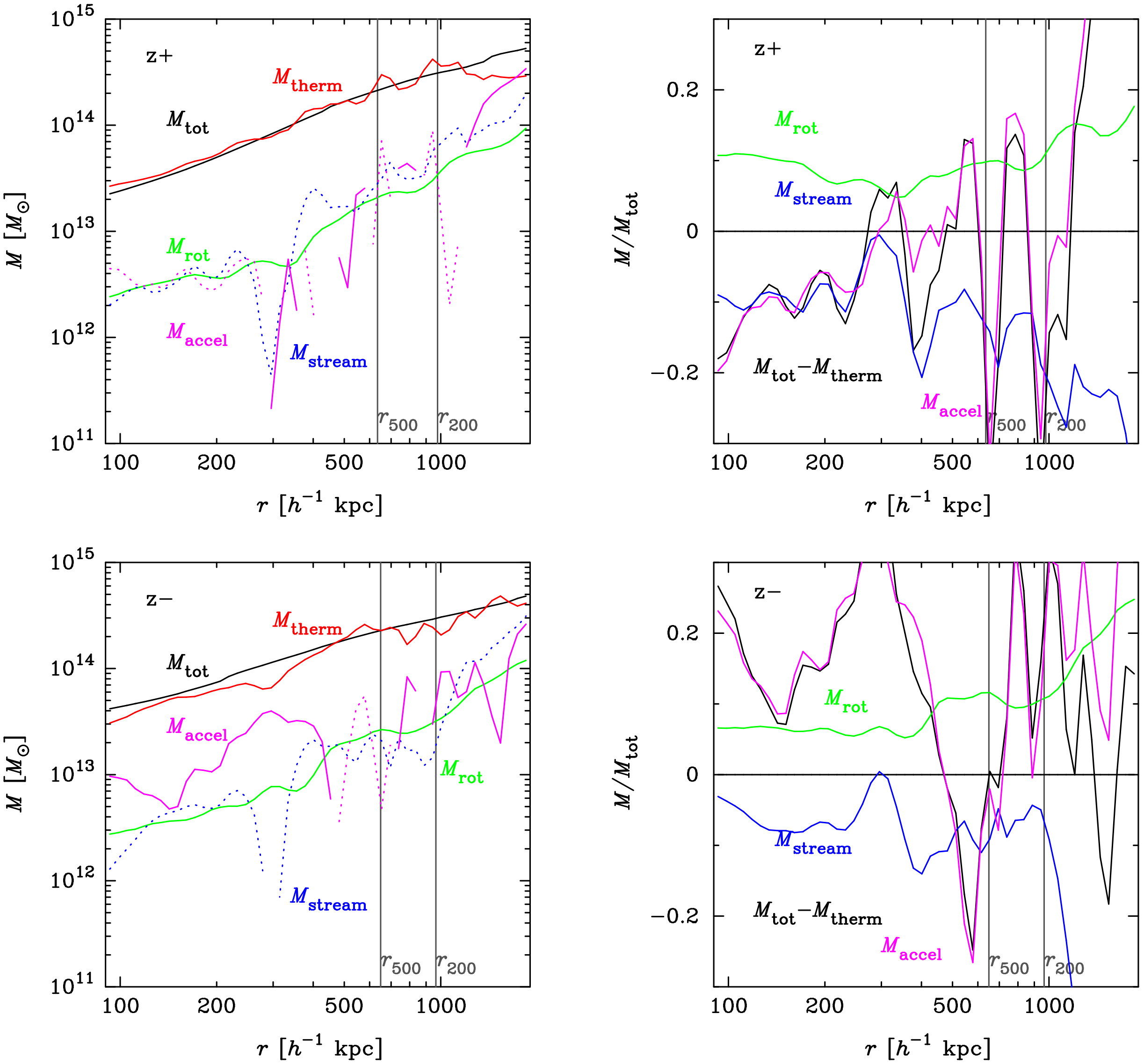

FIG. 6.— Same as Figure 5, but for the clusters "z+" (top) and "z-" (bottom).

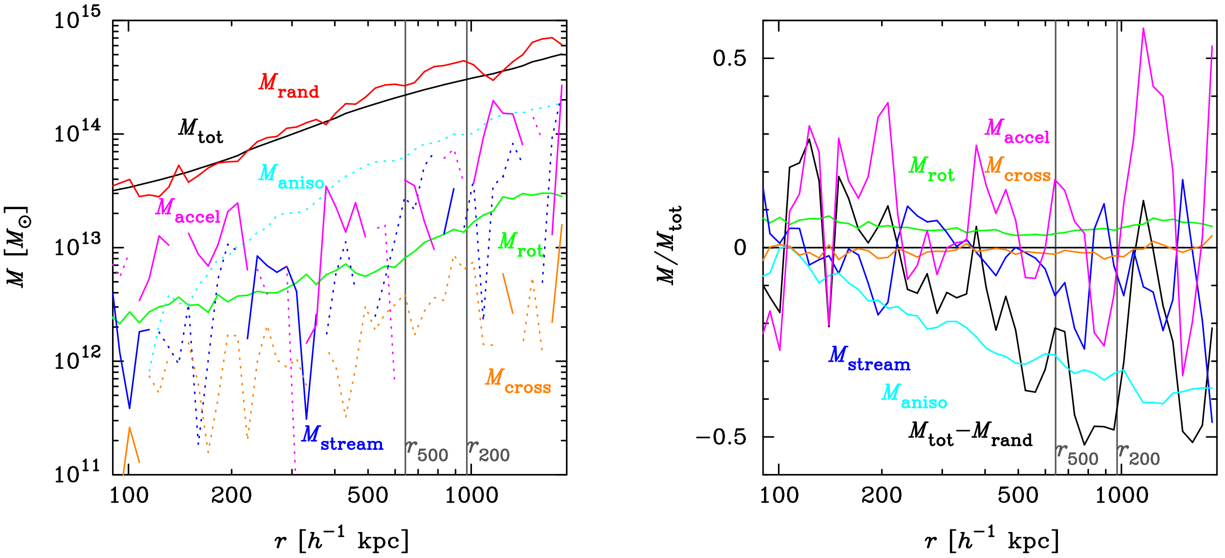

FIG. 7.— The *effective* mass terms in Equation (B3) for the dark matter in the simulated cluster are shown in the left panel: $M_{\rm tot}$ (black), $M_{\rm rand}$ (red), $M_{\rm rot}$ (green), $M_{\rm stream}$ (blue), $M_{\rm aniso}$ (cyan), $M_{\rm cross}$ (orange) and $M_{\rm accel}$ (magenta). Here $M_{\rm accel}$ is calculated by $M_{\rm accel} = M_{\rm tot} - M_{\rm rand} - M_{\rm rot} - M_{\rm stream} - M_{\rm aniso} - M_{\rm cross}$. Dotted line means that its sign is inverted. Ratios of mass terms to $M_{\rm tot}$ are shown in the right panel; The black line shows $(M_{\rm tot} - M_{\rm rand})/M_{\rm tot}$ and other mass terms are colored in the same colors as the left panel.

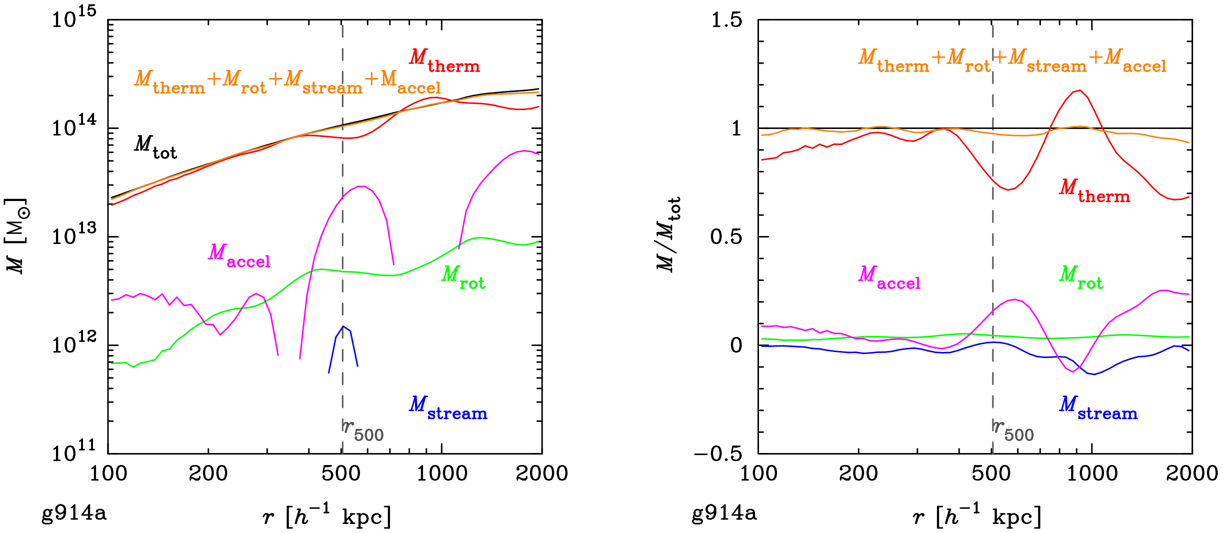

FIG. 8.— The *effective* mass terms in Equation (4) for the cluster g914a from the SPH simulation are shown in the left panel: $M_{\rm tot}$ (black), $M_{\rm therm}$ (red), $M_{\rm rot}$ (green), $M_{\rm stream}$ (blue), $M_{\rm aniso}$ (cyan), $M_{\rm cross}$ (orange) and $M_{\rm accel}$ (magenta). It also shows the sum $M_{\rm therm} + M_{\rm rot} + M_{\rm stream} + M_{\rm accel}$ in orange. Here $M_{\rm accel}$ is calculated using the acceleration data, not $M_{\rm accel} = M_{\rm tot} - M_{\rm therm} - M_{\rm rot} - M_{\rm stream}$. Ratios of mass terms to $M_{\rm tot}$ are shown in the right panel. The color-coding is the same as the left panel. The analysis is performed on the 60 logarithmically equal radial bins.